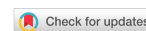


Research Article

Open Access



Theoretical design of dendrite-free zinc anode through intrinsic descriptors from symbolic regression

Mengde Kang, Kai Huang*, Jiahui Li, Honglai Liu, Cheng Lian*

State Key Laboratory of Chemical Engineering, School of Chemistry and Molecular Engineering, East China University of Science and Technology, Shanghai 200237, China.

* **Correspondence to:** Dr. Kai Huang, Prof. Cheng Lian, State Key Laboratory of Chemical Engineering, School of Chemistry and Molecular Engineering, East China University of Science and Technology, No. 130, Meilong Road, Xuhui District, Shanghai, China. E-mail: hk0537@ecust.edu.cn; liancheng@ecust.edu.cn

How to cite this article: Kang M, Huang K, Li J, Liu H, Lian C. Theoretical design of dendrite-free zinc anode through intrinsic descriptors from symbolic regression. *J Mater Inf* 2024;4:6. <https://dx.doi.org/10.20517/jmi.2023.42>

Received: 31 Dec 2023 **First Decision:** 16 Apr 2024 **Revised:** 8 May 2024 **Accepted:** 22 May 2024 **Published:** 27 May 2024

Academic Editors: Xingjun Liu, Lei Zhang **Copy Editor:** Pei-Yun Wang **Production Editor:** Pei-Yun Wang

Abstract

The growth of zinc dendrites limits the practical application of zinc ion batteries, which can be effectively suppressed by surface doping. Herein, the density functional theory combined with symbolic regression algorithm had been used to study the growth of zinc nuclei on 22 single atom-doped surfaces. The results indicate that the doping surfaces with convex structure can suppress the zinc dendrite growth because of the weak adsorption energy and low diffusion activation energy of zinc atoms. Moreover, the diffusion activation energy and the orientation of zinc nucleation depend on the adsorption energy of the first zinc atom. The larger the adsorption energy, the greater the diffusion barrier of zinc atoms and the greater the tendency for vertical growth of zinc nuclei. Therefore, the symbolic regression algorithm was utilized to identify the relationship between the adsorption energy of the first zinc atom and the properties of the doped atom. It was found that the radius and d-band center of doped atoms are key factors affecting the adsorption energy of the first zinc atom, and the doped atom with large atom radius and low d-band center can inhibit the zinc dendrite growth. Finally, the Al, Ag, Cd, In, Sn, Au, Hg, Tl, and Bi atoms are screened out to be the promising doping single atoms that can suppress the zinc dendrite growth.

Keywords: Surface doping, adsorption energy, diffusion activation energy, zinc nucleation, symbolic regression



© The Author(s) 2024. **Open Access** This article is licensed under a Creative Commons Attribution 4.0 International License (<https://creativecommons.org/licenses/by/4.0/>), which permits unrestricted use, sharing, adaptation, distribution and reproduction in any medium or format, for any purpose, even commercially, as long as you give appropriate credit to the original author(s) and the source, provide a link to the Creative Commons license, and indicate if changes were made.



INTRODUCTION

The mass consumption of fossil fuels has caused a rapid increase in demand for high-performance energy storage devices^[1,2]. Electrochemical energy storage devices, such as lithium (LIBs) and zinc ion batteries (ZIBs), have received significant attention in the field of energy storage^[3]. Although LIBs have been widely used in various portable electronic devices and electric vehicles, they still cannot satisfy the demand for high-energy consumption due to the low theoretical capacity of graphite anodes ($372 \text{ mAh}\cdot\text{g}^{-1}$)^[4,5]. Compared to them, ZIBs have many advantages such as low cost, high compatibility, environment friendliness, and high theoretical capacity ($820 \text{ mAh}\cdot\text{g}^{-1}$)^[6-9], considered as a promising alternative to LIBs^[7]. However, they also face issues with dendrite growth, which decreases battery efficiency and capacity^[8,10-12]. The Young's modulus (Y) of zinc is much higher than other alkali metals ($Y_{\text{Zn}} \approx 108 \text{ GPa}$; $Y_{\text{Li}} \approx 5 \text{ GPa}$; $Y_{\text{Na}} \approx 10 \text{ GPa}$)^[13], which means that zinc dendrites grow more easily than lithium or sodium dendrites. Uncontrollable zinc dendritic growth ultimately leads to the direct contact between the anode and cathode, causing a short circuit in ZIBs^[14].

Two effective methods can inhibit the zinc dendrite growth based on the previous studies: (a) adding electrolyte additives^[15-18] and (b) modifying the electrode surface^[8,9,19,20]. For the former, Polyethylene glycol^[21] in organic additives and inorganic salts (Bi^{3+} ^[22] and Pd^{2+} ^[23]) in polar additives have been used to regulate the surface current distribution of electrodes, achieving the goal of inhibiting the zinc dendrite growth. Another method is modifying the anode electrode surface by doped heteroatom^[8], including Al^[24,25], Sn^[26], Ag^[27], Hg^[28], and In^[29], which can provide a large number of nucleation sites to induce uniform deposition^[30,31] or reduce the energy consumption of ion desolvation and the energy barrier for zinc nucleus^[22,32,33]. Especially on the In-doped surface, zinc atoms tend to deposit around the In area, which inhibits zinc deposition, and may even form porous structures, increasing the tolerance of zinc dendrites. More importantly, doping aims to increase the number of Zn ions on the electrode surface, generating more effective nucleus sites^[34]. Surface doping can promote the uniform distribution of interface ions and electric fields and inhibit the growth of zinc dendrites^[9].

The encouraging results in the experiment require an explanation of the mechanism. The adsorption and diffusion behavior of zinc atoms on the electrode surface plays a crucial role in the zinc dendrite growth of ZIBs^[35]. At present, theoretical research in the zinc dendrite growth on doping surfaces only focuses on the adsorption of one zinc atom on a specific doping surface^[28,36,37]. However, the potential mechanism of inhibiting zinc dendrite growth on the zinc doping surface has not been systematically studied. At present, machine learning (ML) is widely used in chemistry because of its learning ability, and it is necessary to use it to summarize and predict battery performance^[38,39].

This work used the density functional theory (DFT) calculations to study the doping surface formation (22 types of doped heteroatoms) and the adsorption and diffusion of zinc atoms on these doping surfaces. The formation energy was used to evaluate the difficulty of forming a doping surface. The adsorption energy, interaction energy, and diffusion activation energy (E_b) of zinc atoms on the doping surface were calculated to assess their nucleation capability. Finally, doping atoms that can effectively inhibit the growth of zinc dendrites were screened out. In order to predict adsorption energy, the symbolic regression (SR) method^[40-42] studied the mathematical relationship between various influencing factors and adsorption energy, promoting the rapid screening of doping atoms to inhibit zinc dendrite growth. We hope our results can provide valuable insights for designing the dendrite-free anode materials of ZIBs.

MATERIALS AND METHODS

All DFT calculations were conducted using the plane-wave-based Vienna Ab initio Simulation Package (VASP)^[43-46]. The projector augmented wave (PAW) pseudopotential described the ionic cores^[47,48]. The Perdew-Burke-Ernzerhof (PBE) functional constructed the exchange and correlation energy^[47]. The kinetic cutoff energy was set to 500 eV. For the calculations of geometry optimization and charge property, a $4 \times 4 \times 1$ k-point mesh based on the Monkhorst-Pack scheme^[49] was used with a 500 eV cutoff energy. For the d-band center calculations and all the adsorption energy computations, a $5 \times 5 \times 1$ Monkhorst-Pack k-point grid was employed. The convergence condition of geometry optimization was set to 10^{-5} eV and 0.01 eV/Å.

Existing experiments have proven that zinc ions exhibit a strong trend of sheet-like deposition during electrodeposition. This means that the deposition of zinc is related to the densest packing plane (002) exposed by the hexagonal close packed structure with low thermodynamic free energy^[50,51]. Therefore, the Zn(002) face was cleaved and doped heteroatom as the substrate to simulate the adsorption and diffusion of zinc atoms on these surfaces. A 4×4 supercell of the Zn(002) face, measuring $10.7 \text{ \AA} \times 10.7 \text{ \AA}$ and containing three layers of 48 zinc atoms, was constructed. To avoid the influence of periodic structural interactions, a 20 Å vacuum layer was constructed in the z-direction. The doping surfaces were constructed by replacing one zinc atom on the Zn(002) face with a heteroatom. All the standard crystal structures and properties of elements were adopted from the Material Project^[52].

To ensure the conductivity of the doping surfaces, the metal elements were selected as dopant atoms. Then, the elements (Al^[25], Ag^[27], In^[29], Sn^[26], Au^[53], Hg^[28], and Bi^[22]), which are reported in the existing literature to inhibit the zinc dendrite growth, were chosen. Moreover, those near these reported elements were also considered. These adjacent elements are from the same group or period as the reported elements, including Al in the third period; Sc, Ti, V, Cr, Mn, Fe, Co, Ni, Cu, Ga, and Ge in the fourth period; Pd, Ag, Cd, In, and Sn in the fifth period; and Pt, Au, Hg, Tl, Pb, and Bi in the sixth period.

The formation energy of doping surfaces (E_f) was calculated by

$$E_f = E_{doped} - E_{pristine} + \mu_{Zn} - \mu_x \quad (1)$$

where E_{doped} is the total energy of the system when the zinc atom was replaced by a heteroatom, and $E_{pristine}$ is the energy of the original Zn(002) face. μ_{Zn} and μ_x are the chemical potential of the zinc and doping atoms, respectively. All the μ_x were calculated based on the naturally occurring bulk and the lowest energy crystal structure can be obtained in the Materials Project material library. The chemical potential of a single atom is calculated by

$$\mu_x = \frac{\mu_{cell}}{n} \quad (2)$$

where μ_{cell} is the total chemical potential of the most stable crystal structure, and n is the number of doping atoms in the crystal structures.

The adsorption energies (E_{abl}) of one zinc atom on the Zn(002) face and doped-Zn(002) face were calculated by:

$$E_{ab1} = E_{doped+Zn} - E_{doped} - \mu_{Zn} \quad (3)$$

where $E_{doped+Zn}$ represents the energy of the first single zinc atom adsorbed on the doping surfaces.

Similarly, the adsorption energy of the second zinc atom is given by:

$$E_{ab2} = E_{doped+2Zn} - E_{doped+Zn} - \mu_{Zn} \quad (4)$$

where $E_{doped+2Zn}$ is the total energy of the structure after absorbing two zinc atoms.

The surface energy profiles [$E_s(x, y)$] were calculated to describe the diffusion of zinc atoms on the Zn(002) face and the doped-Zn(002) face. The x , y , and z are the coordinates of the adsorbed zinc atom. The $E_s(x, y)$ is defined by the maximum adsorption energy when the x and y coordinates are fixed, which is given by:

$$E_s(x, y) = \max \{E_{ad} = (x = x_0, y = y_0, z)\} \quad (5)$$

The E_b is the difference between the minimum $E_s(x, y)$ and adsorption energy of one zinc atom (E_{ab1}), calculated by^[11]:

$$E_b = \min \{E_s(x, y)\} - E_{ab1} \quad (6)$$

To measure the impact of various parameters on the adsorption of one zinc atom, ML evaluates the importance of factors. SR is an interpretable ML model and can express the trained ML model in mathematical expressions^[42]. Therefore, it can be used in materials science to search for characteristic descriptors of a certain material property. This paper used this method to construct a new descriptor to predict the first zinc atom adsorption energy on different doping surfaces by HeuristicLab^[53].

RESULTS AND DISCUSSION

The formation of doping surface

The formation energy of 22 types doping surfaces and relationship between the formation energy of atom-doped surfaces and the chemical potential of doped elements are shown in [Figure 1A](#). It is found that as the atomic chemical potential increases, the formation energy grows. The reason is that a simple substance composed of elements with large chemical potential is stable, and it is difficult to form a doped surface. However, the formation energies of surfaces doped with Pt, Au, and Pd are contrary to the relationship. To analyze the cause of the anomaly, the Bader charge was calculated. And these atoms get large charge ($> 0.5 |e|$) because of large electronegativity of Pt ($\chi_{Pt} = 2.2$), Au ($\chi_{Au} = 2.4$), and Pd ($\chi_{Pd} = 2.2$), causing strong interaction between the surface and doping atom and formation energy decrease. The Al (-0.176 eV)^[23], Hg (-0.348 eV)^[28] and Ag (-0.396 eV)^[27] doping surfaces exhibit the negative formation energies and are thermodynamically easy to form, which has already been proven in experimental studies. It can be clearly seen that the transition elements in the third period (Ti, V, Cr, Mn, Fe, and Co) exhibit positive formation energy because of their higher atomic chemical potential than that of other elements. Therefore, these elements with positive formation energy will not be considered in the following research.

Different doping surfaces show varying geometric structures, which are related to the radius of doped elements. According to geometric structure, these structures can be divided into three categories [[Figure 1B](#)]: flat, concave, and convex surfaces. The structure and charge distribution of flat doping surface

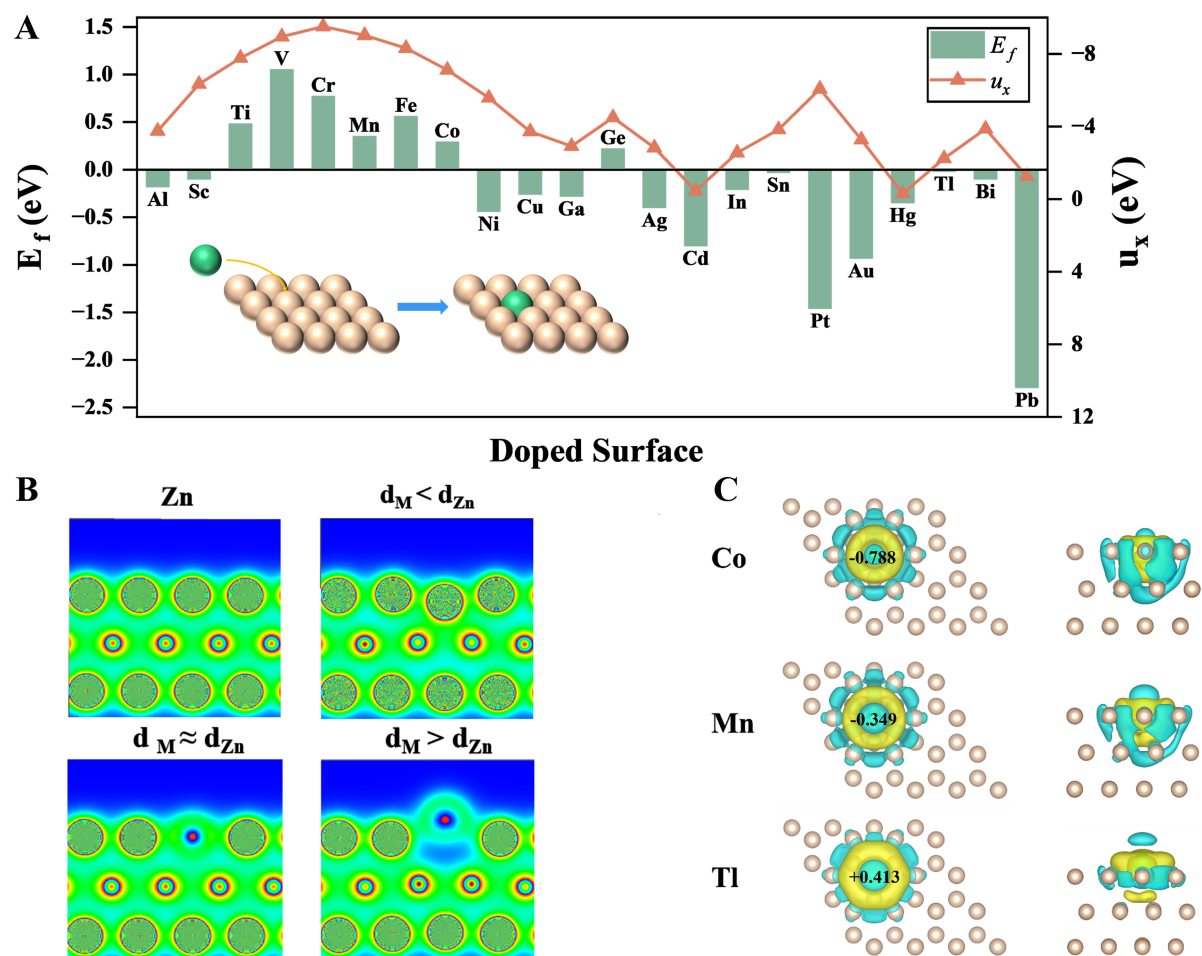


Figure 1. The formation of doping surface: (A) the formation energy of doping surfaces and the atomic chemical potential of doping elements; (B) the geometric structure of doping surfaces; (C) the charge density differences and Bader charge of doping surface. The green and yellow regions represent the electron accumulation and depletion, respectively, and the isosurface value is $\pm 0.001 \text{ e/bohr}^3$.

(Mn, V, Pt, and Pd) are similar to the Zn(002) face, owing to the similarity in radii between the doped atoms and zinc atom ($d_{Zn} = 1.37 \text{ \AA}$). When the radius of the doped atoms (d_M) is smaller than that of the zinc atoms, such as Ni ($d_{Ni} = 1.25 \text{ \AA}$), Cu ($d_{Cu} = 1.28 \text{ \AA}$), and Ga ($d_{Ga} = 1.22 \text{ \AA}$), the doped atoms will be trapped within the surface and form a concave surface. It may cause a strong deposition trend of zinc atoms on the doping surfaces. On the contrary, if the radius of doped atoms is larger than that of the zinc atom, the doping site will form a convex surface structure, potentially weakening the interaction between the zinc atoms and the surface and promoting uniform Zn deposition.

The charge density differences and Bader charge analysis of the doping surface Zn(002) face were calculated [Figure 1C]. An electron-rich region forms around the doped atom due to charge transfer to the adjacent zinc atoms. The regions affected by doping atoms are relatively small (Mn: 3.75 \AA , and Tl: 4.54 \AA). The Bader charge analysis shows that the direction of charge transfer depends on the electronegativity of the doped atom. The doped atom with high electronegativity will gain negative charge from the zinc atom. For example, compared to the zinc atom ($\chi_{Zn} = 1.65$), the Au atom ($\chi_{Au} = 2.4$) can obtain electrons of $0.749 |e|$, while the Sc atom ($\chi_{Sc} = 1.36$) loses electrons of $1.35 |e|$. Conversely, the electrons will transfer from doped atoms with low electronegativity to contiguous zinc atoms [Supplementary Figure 1]. The difference in

surface charge will change surface energy. After doping heteroatom, the surface energy of the doping surface is reduced, which may cause the adsorption and aggregation of zinc atoms at the doping site^[54].

The adsorption and diffusion of single zinc atom

The adsorption of zinc atoms on the surface is one of the key factors for zinc nuclei. The higher the adsorption energy, the easier the zinc nucleus growth^[54]. For the doping surface, four different adsorption sites of zinc atoms on the doping surface were considered, as presented in [Figure 2A](#): (1) top site of doped atoms (TD); (2) top site of zinc atoms near the doped atom (TZ); (3) bridge site between doped and zinc atoms (B); (4) vacancies formed between doped and zinc atoms (V). The adsorption energy is listed in [Supplementary Tables 1-3](#). It is shown that zinc atoms tend to adsorb at the V site on the Zn(002) face due to the hexagonal close-packed structure of zinc. On most single atom doping surfaces (except for Ga, Sn), they generally adsorb at the TD site [[Supplementary Figure 2](#)], which owns the maximum change in the surface energy, meaning that the TD site is the minimum value of the potential energy surface [[Figure 2A](#)]^[54]. However, on the surfaces doped with Ga and Sn, they adsorb at the TZ site, suggesting that these doped atoms may prevent their adsorption. When the Ga (or Sn) atoms are uniformly distributed on the Zn(002) face, the uniform adsorption of zinc atoms may prevent aggregation and the formation of zinc dendrites. The surface doping with Sn atoms has been experimentally proven to inhibit dendritic growth, indicating that this repulsive effect may inhibit the zinc nuclei growth^[26]. Meanwhile, for surfaces doped with large-radius atoms, the optimal adsorption site is the B site. This may be due to doping atoms with a large radius significantly weakening the interaction between adsorbed zinc atoms and the surface, resulting in a greater decrease in the adsorption energy at the TD site. The zinc atoms adsorbed at the V site are in direct contact with the surface and the doping atoms, increasing the adsorption energy at this site. Additionally, the calculation of the diffusion barrier later proved the formation of a potential energy well at the V site. Obviously, the zinc atom on most doping surfaces has a smaller adsorption energy than that on the Zn(002) face ($E_{ad1} = -0.34$ eV) due to decreased surface energy caused by doping [[Figure 2B](#)]. For Sc, Ni and Pt-doped surfaces, the adsorption energy of zinc atoms ($E_{ad1-Sc} = -0.416$ eV, $E_{ad1-Ni} = -0.525$ eV, $E_{ad1-Pt} = -0.470$ eV) is stronger than that on Zn(002) face, which may be detrimental to their desorption and zinc dendrites formation. A strong adsorption energy will hinder the inhibition of zinc nuclei growth. The surfaces doped with Sc, Ni, and Pt have a larger adsorption energy for zinc atoms than the Zn(002) face, indicating that these three types of doping surfaces are unsuitable for the anode materials of ZIBs. The doped atoms will suppress the adsorption of zinc at the doped site. When a small number of doping sites are uniformly distributed, zinc atoms adsorbed away from the doped site, causing the uniform deposition. Additionally, a small amount of surface doping will not compromise the overall performance of the battery. On the contrary, it may even improve the cycle life^[9,22].

Another key factor for zinc nuclei is the diffusion of zinc atoms on the surface^[11]. The two-dimensional and three-dimensional surface energy profiles of zinc atom diffusion are shown in [Figure 2C](#). The results show that the surface energy variation of zinc atom diffusion is related to the surface structure. Thus, three doping surfaces were shown in [Figure 2D](#), each not only satisfying the low adsorption energy of zinc atoms but also possessing different geometric structures. On the surface doped with Co, Mn and Tl, representing the three geometric structures, the Bader charge transfer of the adsorbed zinc atoms decreases with the shortening of the distance between the zinc and the surface, reflecting the influence of the surface binding structure on the adsorption of zinc atoms. These findings demonstrate a correlation between the variation of surface energy of zinc atom diffusion and the surface structure. For the Zn(002) face, the maximum adsorption energy occurs at V sites on the surface. Meanwhile, the adsorption energy of the TZ site is the smallest, which is consistent with the results of optimizing the adsorption structure. The adsorption energy of zinc atoms at the B site exhibits a saddle point in surface energy profiles, indicating the optimal diffusion path for zinc atoms on the Zn(002) face: V-B-V site. The E_b of zinc atoms along this path is 0.005 eV, which

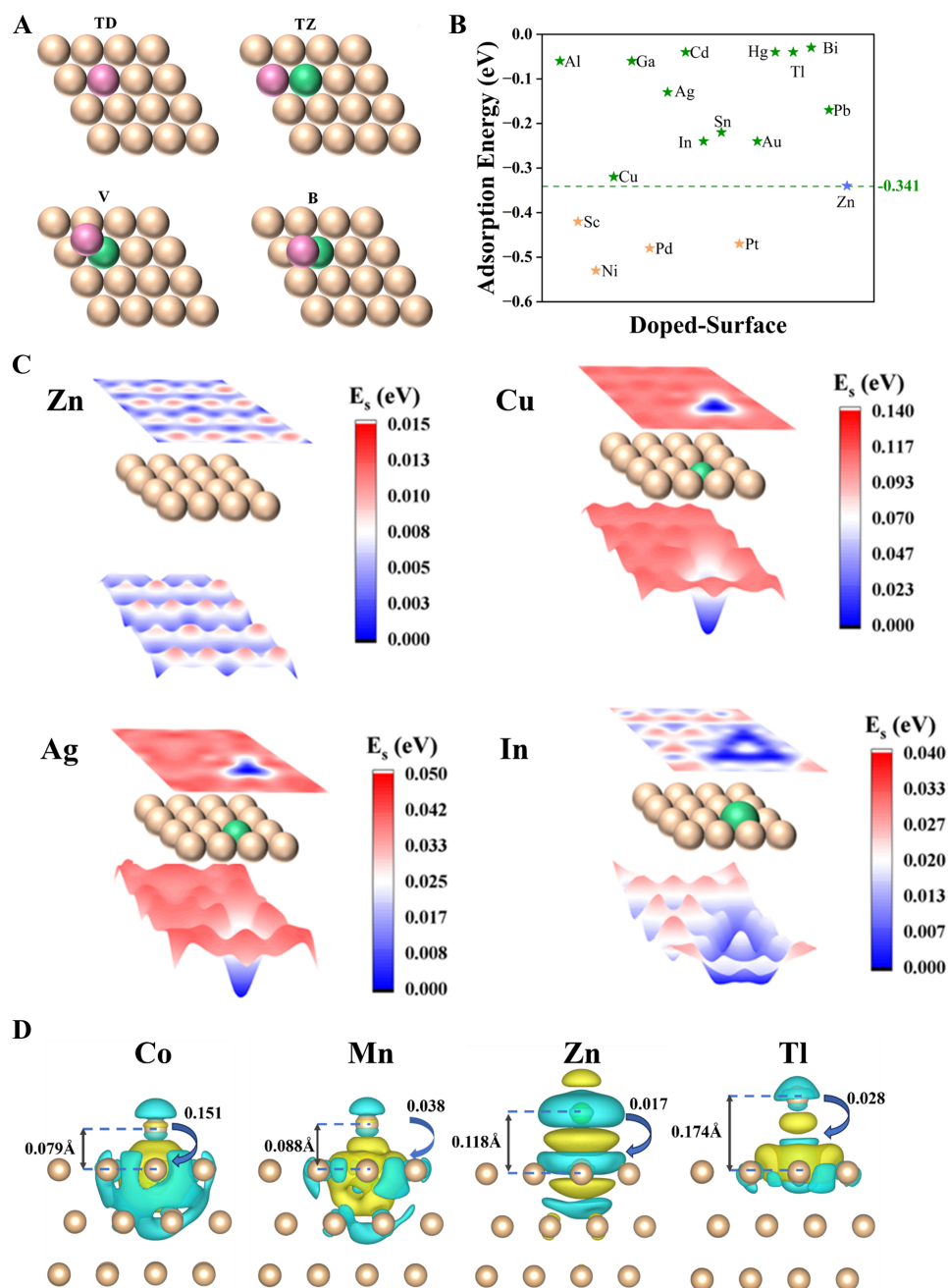


Figure 2. The adsorption and diffusion of one zinc atom on doping surface: (A) four adsorption sites of zinc atom; (B) the maximum adsorption energy of Zn atom; (C) the surface energy profiles of Zn self-diffusion on Zn, Cu, Ag and In-doped surfaces; (D) the charge density differences, Bader charge and adsorption distance of zinc atom on the Co, Mn, Zn, and Tl-doped surfaces. The green and red regions represent the electron accumulation and depletion, respectively, and the isosurface value is $\pm 0.0001 \text{ e}/\text{bohr}^3$.

is similar to the results in the literature^[55], indicating the small diffusion resistance of zinc atoms on the Zn(002) face.

For concave and flat doping surfaces, the maximum adsorption energy occurs at TD sites. Due to the influence of the doped atoms, a triangular potential well is formed on the surface. Similar to the Zn(002) face, saddle points appear at the B sites between doped and zinc atoms. The E_b of zinc atoms is positively

correlated with their maximum adsorption energy. The diffusion activation energies of Cu- ($E_{ad1-Cu} = -0.323$ eV) and Ag-doped surfaces ($E_{ad1-Ag} = -0.135$ eV) are 0.101 and 0.034 eV, respectively. The surface energy profiles show that the diffusion of zinc atoms leaving the potential well requires higher energy than that of zinc atoms on the Zn(002) face. Therefore, for the concave and flat doping surfaces, zinc atoms are attracted into the potential well by doped atoms, forming a stable zinc nucleus. For convex doping surfaces, the V sites show the strongest adsorption energy, and three optimal adsorption sites are formed around the doped atoms. For the E_d of zinc atoms leaving the potential well, the E_d of convex doping surfaces is lower than that of concave and flat doping surfaces. The E_b far away from doping sites is close to that on the Zn(002) face. The reason is that the large radius of doped atoms weakens the interaction between the adsorbed zinc atom at the TD site on the doping surface. It means that doped atoms with a large radius will not affect the diffusion of zinc atoms. For example, the E_b of zinc atoms on the In-doped surface is 0.009 eV, similar to the E_b on the Zn(002) face.

In conclusion, the strong adsorption energy of zinc atoms on Sc, Ni and Pt-doped surfaces may lead to the growth of zinc dendrites. Additionally, the concave and flat doping surface will attract zinc atoms into the potential well and form stable zinc nuclei, causing the dendrite growth. The convex doping surface may effectively inhibit this growth.

The adsorption of multiple zinc atoms

Zinc nucleation results from the aggregation of multiple zinc atoms on the surface. Therefore, the adsorption of these atoms on the Zn(002) face and doping surface was studied in this part. Based on the adsorption of one zinc atom, four adsorption sites of the second adsorbed zinc atom were designed [Figure 3A]: top, adjacent, vacancy, and bridge sites. For the Zn(002) face, zinc atoms preferentially adsorb at vacancies, which is related to their maximum adsorption energy on this surface. The adsorption energy of the second zinc atom, higher than that of the first ($E_{ad2-Zn} = -0.960$ eV > $E_{ad1-Zn} = -0.341$ eV), underscores the importance of the adsorption of the first atom in initiating zinc nucleation.

The adsorption behavior of the second zinc atom on the doping surfaces depends on the geometric structure of the doping surfaces [Figure 3B]. For flat or concave surfaces ($d_M \leq d_{Zn}$), the second zinc atom will preferentially adsorb at vacancies or bridge sites on the doping surface. The adsorption height (the distance between the zinc atom and doping surface) of the second zinc atom is similar to the first. The adsorption energy of the second zinc atom is significantly enhanced, mirroring the phenomenon observed on the Zn(002) face. On a convex surface, the first zinc atom always adsorbs at the top site of the doped atom, while the second adsorbs on the site near the doped atom. The adsorption height of the second zinc atom is lower than the first one. The simulation results also confirm that the doped site will form a potential well and attract zinc atoms.

Afterward, two adsorption trends were designed to investigate the orientation of zinc nucleation: parallel and vertical adsorption [Figure 3C]. The parallel adsorption may cause uniform deposition of zinc atoms on the surface, and the vertical adsorption may cause the zinc dendrite growth. Calculation results show that all surfaces (except for the Al-doped surface) exhibit stronger adsorption energies for parallel than for vertical adsorption, indicating that zinc atoms on these surfaces tend to deposit uniformly. However, vertical adsorption energies of these surfaces are also negative, which means that zinc dendrites may still grow. For example, the Cu-doped surface has a higher E_{ad2-v} of the vertical adsorption (-0.37 eV) than the Zn(002) face (-0.24 eV), proving that zinc dendrites are easier to grow on the Cu-doped surfaces than on the Zn(002) face. The experimental studies of previous literature also prove that Cu atoms exhibit depolarization on the zinc surface, leading to the growth of numerous leaf-like dendrites^[15].

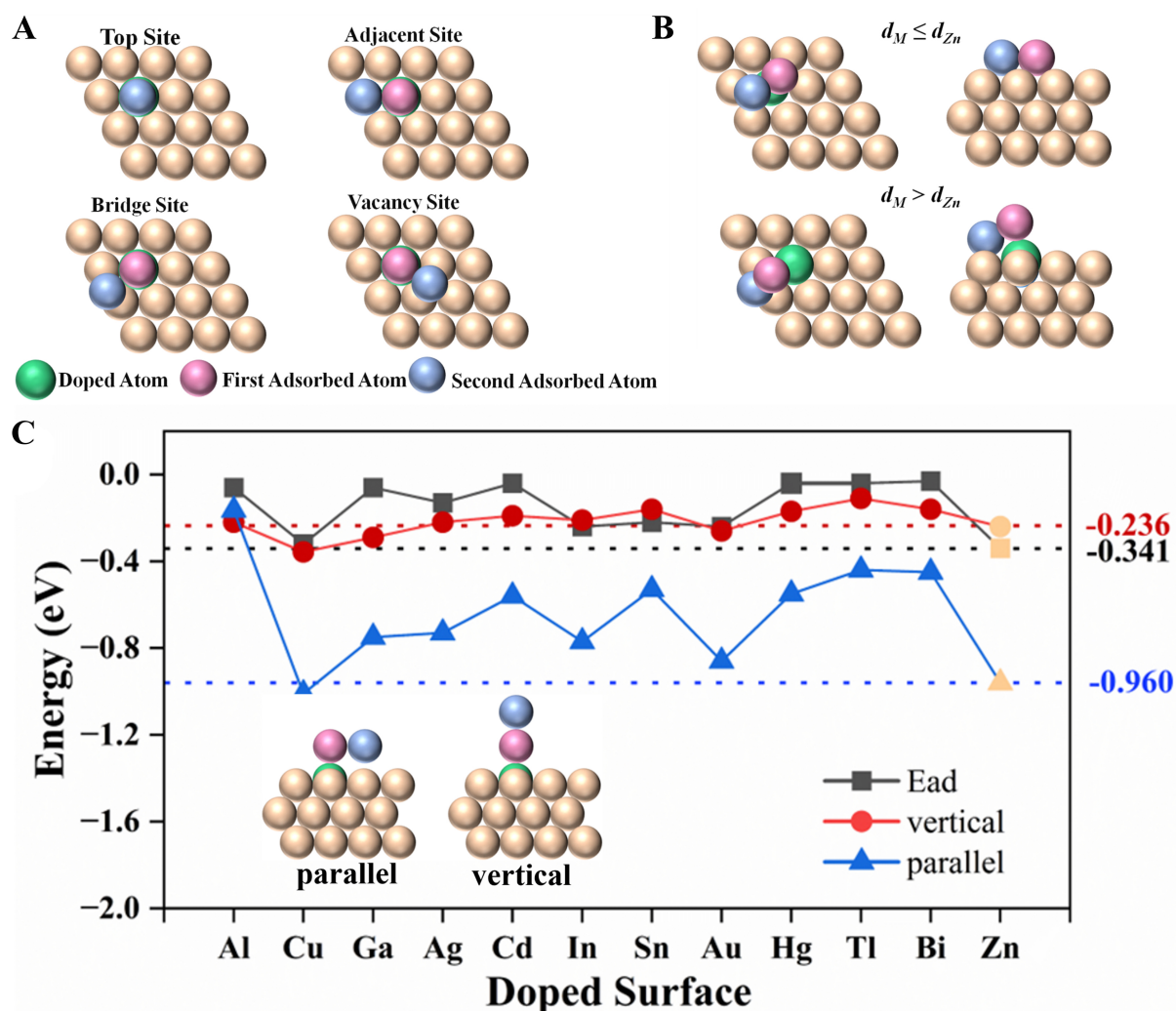


Figure 3. Adsorption of multiple zinc atoms on doping surface: (A) the adsorption site of two Zn atoms; (B) the adsorption behavior of two zinc atoms on different doping surfaces; (C) the first adsorption energy, the adsorption energy of parallel and vertical adsorption on the doping surface.

Additionally, to further investigate the orientation of zinc nucleation, multiple zinc atoms ($n = 3, 4$), varying in heights and sites, were placed on the Zn(002) face. After geometry optimization, it was found that zinc atoms will vertically stack on the surface, and the adsorption energy is -1.08 eV, indicating that vertical growth of zinc nucleus can occur thermodynamically [Supplementary Figure 3]. Similarly, they have a trend of vertical stacking on doping surfaces, and the adsorption energies of the second, third, and fourth zinc atoms gradually increase. This implies that once vertical stacking occurs, the subsequent adsorbed zinc atoms will grow uncontrollably in the vertical direction, which may directly lead to the growth of dendrites. Interestingly, the adsorption energies of subsequent zinc atoms are related to the adsorption energy of the first zinc atom; the weaker the first adsorption energy, the smaller the vertical adsorption energy, and the smaller the trend of vertical stacking^[56]. doping surfaces with larger-radius atoms exhibit small first adsorption energy, indicating that these surfaces can inhibit the zinc dendrite growth.

To further investigate the interaction between vertically adsorbed atoms, their Bader charge is calculated. Obviously, as the number of adsorbed zinc atoms increases, the atom closest to the surface loses more

charge, which strengthens its interaction with the surface. This contributes to the stability of this vertical adsorption configuration. The charge transition of the vertical adsorption on the zinc metal surface shows that the interaction between zinc atoms and surfaces raised with the height of zinc atoms. On the contrary, the charge transfer of the doped surface zinc atoms decreases as the height of the atom increases, which is the reason for the smaller tendency of vertical adsorption on the doped surfaces [Supplementary Figure 4].

In conclusion, a vertical growth trend of zinc nuclei existed on the electrode surface. Correspondingly, the surface doped with large-radius atoms has weaker vertical adsorption energy and lower diffusion energy barrier than those doped with small-radius atoms, which can effectively inhibit the growth of zinc dendrites. Among doping atoms, the surface doped with Cu and Ga shows a stronger trend of vertical zinc nuclei growth, which is not conducive to inhibiting this growth. These findings demonstrate that doping the surfaces with Al, Ag, Cd, In, Sn, Au, Hg, Tl, and Bi can effectively inhibit dendrite growth. Among these elements, Al, Ag, In, Sn, Au, Hg, and Bi have been proven experimentally that these elements can induce uniform zinc deposition^[21,22,26-29,57]. And the Bi-doped-surface^[22] with the minimum adsorption energy of zinc atom may have the best zinc dendrite-inhibiting effect. However, there are few reports on the work of doping with Cd and Tl, and our results can provide theoretical guidance for future experimental studies.

Because zinc-based batteries commonly use water as the electrolyte, water molecules may affect the deposition of zinc atoms on the surface. Therefore, the adsorption energies of water molecules on the doping surfaces were calculated in Supplementary Figure 5. In all surfaces except for the Au-doped surface, the adsorption energy of water molecules is negative, indicating that they can stably adsorb on doping surfaces. The positive adsorption energy of the Au-doped surface may be due to the low metal reactivity of Au, leading to weak interaction with oxygen. For the doping surfaces that can inhibit zinc dendrite growth in experiments, the adsorption energy of water molecules is smaller than on the zinc metal surface. These results prove that doped atoms can weaken the adsorption energy of water molecules and inhibit the hydrogen evolution reaction (HER).

Explore the descriptors affecting zinc atom adsorption energy

According to the calculation results, for zinc atom diffusion, the E_b is positively correlated with the adsorption energy of one zinc atom. For zinc nucleation, the adsorption of the first zinc atom is the key factor. Therefore, exploring the descriptors affecting adsorption energy of one zinc atom is necessary. Figure 4A-D illustrates the relationship between the adsorption energy and the properties of the doped atom, including radius, electronegativity, d-band center, and charge transfer.

The adsorption energy is negatively correlated with atomic radii [Figure 4A]. Compared with Zn ($R = 1.37 \text{ \AA}$) atoms, the small radius of doped atoms, such as Fe ($R = 1.26 \text{ \AA}$), Cr ($R = 1.29 \text{ \AA}$), and Ni ($R = 1.25 \text{ \AA}$) atoms, may exhibit the strong adsorption energy of zinc atoms. Doped atoms with large radius show the opposite phenomenon (In: $R = 1.67 \text{ \AA}$, Tl: $R = 1.71 \text{ \AA}$, Pb: $R = 1.75 \text{ \AA}$, and Bi: $R = 1.82 \text{ \AA}$). This result arises from the distance alteration between the adsorbed zinc atoms and the doping surface by the doping atoms, thereby diminishing their interaction. However, the trend does not show a good linear relationship ($R^2 = 0.34$), indicating that the radius of doped atoms cannot accurately evaluate the adsorption energy. The d-band center is considered as a good descriptor for the adsorption energy. Therefore, the d-band centers of doped atoms were calculated to correlate the relationship between the d-band center and the adsorption energy, [Figure 4B]. For most doping surfaces, the d-band center exhibits a good linear relationship with adsorption energy, except for Hg, Bi, Tl and Cd-doped surfaces, because their larger atomic radius reduces interactions between the adsorbed zinc atom and the zinc metal surface. The correlation coefficient of the linear relationship is 0.64, meaning that the d-band center cannot describe the adsorption energy separately.

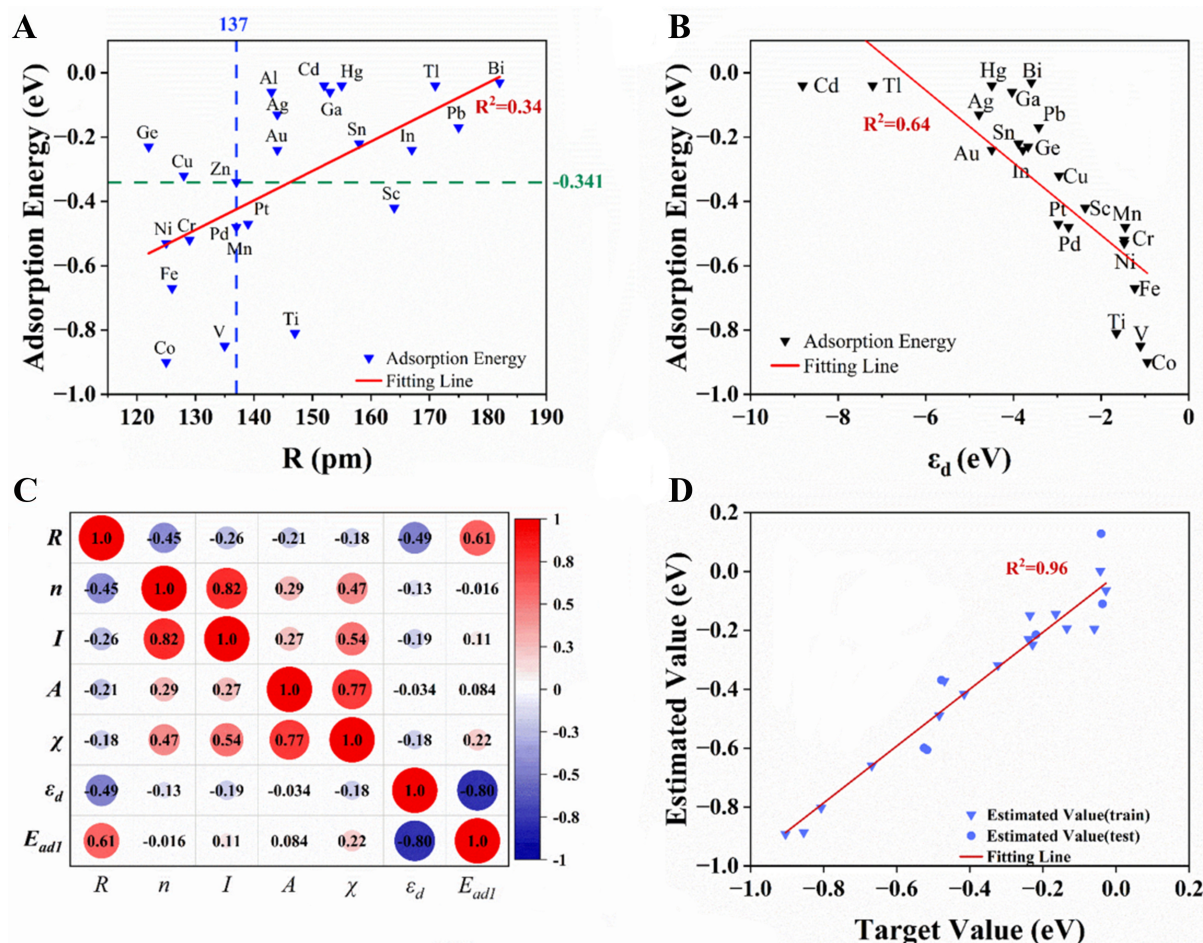


Figure 4. The relationship between the properties of the doped atom and the adsorption energy of E_{ad1} : (A) radii of doped atoms, (B) band center, and (C) the heat maps of various factors used in machine learning; (D) Comparison of calculated E_{ad1} by DFT and estimated E_{ad1} by ML. DFT: Density functional theory; ML: machine learning.

The electronegativity difference between doped and zinc atoms may affect the interaction between the adsorbed zinc atoms and the surface. Accordingly, the correlation between electronegativity of doped atom and adsorption energy was studied in [Supplementary Figure 6](#). Unfortunately, there is no strong correlation between adsorption energy and electronegativity [[Supplementary Figure 6](#)]. For example, the adsorption energy of zinc on Au ($\chi = 2.4$)-doped surfaces is -0.24 eV, weaker than that on Co ($\chi = 1.8$)-doped surfaces (-1.56 eV). With zinc having an electronegativity of 1.65, it can be observed that elements with similar electronegativity to it and a larger atomic radius exhibit lower adsorption energy, while elements with significantly different electronegativity often have greater adsorption energy than the zinc metal surface. To find other descriptors, charge transfer of doped atoms after zinc adsorption was considered [[Supplementary Figure 7](#)], which can show the strength of interaction between the adsorbed zinc atom and the doped atoms. It is shown that there is a trend of stronger interactions as the amount of charge transfer increases. However, the trend does not exhibit a good linear relationship ($R^2 = 0.35$, [Supplementary Figure 7](#)): the adsorption energy of doping surfaces with larger-radius doped atoms appears above the fitted line, indicating weaker interactions than expected; correspondingly, the adsorption energy of doping surfaces with smaller-radius doped atoms appears below the fitted line, indicating stronger adsorption than the expected. The poor linear relationship between charge transfer and adsorption energy since the Bader charge transfer reflects the transfer of charge but does not directly reflect the magnitude of the interaction

forces. Furthermore, the distance between the adsorbed zinc atoms and the surface also affects the magnitude of the interaction forces, resulting in the adsorption energy on surfaces doped with large-radius atoms often smaller than on surfaces doped with small-radius atoms. Therefore, it is difficult to present a linear relationship between them.

The above factors can reflect the trend of adsorption energy change but cannot accurately describe the numerical value of adsorption energy. Therefore, the adsorption of zinc atoms cannot be described by a single physical or chemical property and can be influenced by multiple factors. The heatmap analyzed the correlation between various factors [Figure 4C]. The results show a positive correlation between the radius of doped atoms and the value of adsorption energy (correlation coefficient: 0.61); the d-band center is negatively correlated with the adsorption energy (correlation coefficient: -0.81) due to the negative value of the adsorption energy. The two factors will play an important role in predicting adsorption energy. To accurately describe the adsorption energy of zinc atoms on doping surfaces, ML was used to synthesize the effects of various factors and form a new descriptor.

The data acquisition of ML models is based on the calculated adsorption energy of one zinc atom on the doped surface [Supplementary Table 4], and 25% of the dataset was divided into test sets. In order to identify parameters that may affect adsorption energy, various physical and chemical properties, including electronegativity (χ), valence electrons (n), first ionization energy (I), electron affinity (A), d-band center (ϵ_d), and the ratio of radius between doped atoms and zinc atoms (R), were used to train the SR model. The SR with the genetic program (GPSR) was adopted to find the mathematical formula. These factors were bred, mutated, and evolved to form a new descriptor during the genetic program. The evaluation of the program is determined by Pearson's R , which can reflect the linear relationship between the result predicted by SR models and the calculated adsorption energy by DFT. Both the maximum symbolic expression tree depth and length were set to 35. The arithmetic functions, including addition, subtraction, multiplication, and division, were considered, and power functions, including square, power, square root, root, cube, and cube root, were adopted.

The results of the SR model are presented in the Supplementary Materials. After training, the model depth is 12, and its length is 34. The mean absolute error (MAE) is 0.086 for the test set and 0.036 for the training set. The R^2 values of the training and test sets are 0.966 and 0.873 [Figure 4D], respectively, indicating a good linear relationship between the trained model and calculated data (the criterion is $R^2 > 0.8$). The partial dependence plots [Supplementary Figure 8], show that the adsorption energy increases with the radius ratio and decreases with ϵ_d . The change rate of adsorption energy with radii is smoother than that of the d-band center, indicating that radii have a smaller influence on adsorption energy than the d-band center. ML can analyze the contribution of each factor to the prediction outcome^[58,59]. In the formula of Supplementary Table 4, the impacts of variables ϵ_d , R , A , and χ are 0.876, 0.194, 0.069, and 0.006, respectively, proving that the ϵ_d and R have the greatest impact on adsorption energy, with ϵ_d having the greater impact.

CONCLUSIONS

In this work, the growth mechanism of zinc nuclei on single atom-doped surfaces was studied by calculating the adsorption energy and E_b of zinc atoms. We found that the doping surface with concave geometric structure will enhance the adsorption energy of zinc atoms and lead to an increased trend of vertical zinc nuclei growth. To suppress the vertical growth of zinc nuclei, we selected surfaces doped with nine types of elements: Al, Ag, Cd, In, Sn, Au, Hg, Tl, and Bi, which have thermodynamic stability and parallel growth of zinc nuclei. In addition, the results show that the zinc atom diffusion and zinc nucleation are related to the adsorption energy of the first zinc atom on the surface. Therefore, the SR algorithm was used to explore the

influence of various factors on the adsorption energy. The results indicate that doped atoms with large radius and low d-band centers have weak adsorption energy of zinc atoms, which may inhibit the growth of zinc dendrites. Our work can provide theoretical guidance for the design of a dendrite-free anode of ZIBs.

DECLARATIONS

Authors' contributions

Conceived the idea for scientific research: Huang K, Lian C

Performed the theoretical calculations: Kang M

Assisted in processing the data of DFT calculations: Kang M, Huang K, Lian C

Provided technical support for machine learning and completed data analysis and processing: Kang M, Li J

Wrote the manuscript and finalized it with support: Kang M, Huang K, Li J, Lian C, Liu H

Availability of data and materials

Not applicable.

Financial support and sponsorship

This work was sponsored by the National Key Research and Development Program of China (No. 2022YFA1503501), the National Natural Science Foundation of China (Nos. 22278127, 22308095), the Fundamental Research Funds for the Central Universities (2022ZFH004), the China Postdoctoral Science Foundation (2022M720049), Shanghai Pilot Program for Basic Research (22T01400100-18), and 21C Innovation Laboratory, Contemporary Ampere Technology Ltd by project No. 21C-368 OP-202312.

Conflicts of interest

Lian C is an Editorial Board Member of the *Journal of Materials Informatics*, while the other authors have declared that they have no conflicts of interest.

Ethical approval and consent to participate

Not applicable.

Consent for publication

Not applicable.

Copyright

© The Author(s) 2024.

REFERENCES

1. Shaqsi AZ, Sopian K, Al-hinai A. Review of energy storage services, applications, limitations, and benefits. *Energy Rep* 2020;6:288-306. [DOI](#)
2. Obama B. The irreversible momentum of clean energy. *Science* 2017;355:126-9. [DOI](#) [PubMed](#)
3. Liu Y, Wu X. Review of vanadium-based electrode materials for rechargeable aqueous zinc ion batteries. *J Energy Chem* 2021;56:223-37. [DOI](#)
4. Shu ZX, Mcmillan RS, Murray JJ. Electrochemical intercalation of lithium into graphite. *J Electrochem Soc* 1993;140:922-7. [DOI](#)
5. Li W, Sun X, Yu Y. Si-, Ge-, Sn-based anode materials for lithium-ion batteries: from structure design to electrochemical performance. *Small Methods* 2017;1:1600037. [DOI](#)
6. Wan F, Zhang Y, Zhang L, et al. Reversible oxygen redox chemistry in aqueous zinc-ion batteries. *Angew Chem Int Ed Engl* 2019;58:7062-7. [DOI](#) [PubMed](#)
7. Zhou T, Zhu L, Xie L, et al. Cathode materials for aqueous zinc-ion batteries: a mini review. *J Colloid Interface Sci* 2022;605:828-50. [DOI](#) [PubMed](#)
8. Zuo Y, Wang K, Pei P, et al. Zinc dendrite growth and inhibition strategies. *Mater Today Energy* 2021;20:100692. [DOI](#)
9. Lu W, Xie C, Zhang H, Li X. Inhibition of zinc dendrite growth in zinc-based batteries. *ChemSusChem* 2018;11:3996-4006. [DOI](#) [PubMed](#)

10. Naskar S, Ojha M, Gazi TR, Ghosal P, Deepa M. Dendrite growth inhibition in a V_6O_{13} nanorods based non-aqueous Zn-ion battery by a scalable polycarbazole@Carbon nanotubes overlayer. *Compos Part B Eng* 2023;252:110516. DOI
11. Huang K, Du J, Hu J, et al. Suppressing lithium dendrites by coating MoS_2 with different layer spacings: a multiscale simulation study. *Chem Eng Sci* 2021;244:116795. DOI
12. Yang S, Du H, Li Y, et al. Advances in the structure design of substrate materials for zinc anode of aqueous zinc ion batteries. *Green Energy Environ* 2023;8:1531-52. DOI
13. Meyer N, Xu H, Wax JF. Universality of the shear viscosity of alkali metals. *Phys Rev B* 2017;96:094201. DOI
14. Yang S, Chen A, Tang Z, et al. Regulating the electrochemical reduction kinetics by the steric hindrance effect for a robust Zn metal anode. *Energy Environ Sci* 2024;17:1095-106. DOI
15. Geng M, Northwood DO. Development of advanced rechargeable Ni/MH and Ni/Zn batteries. *Int J Hydrogen Energy* 2003;28:633-6. DOI
16. Chang M, Chen F, Fang N. Analysis of membraneless fuel cell using laminar flow in a Y-shaped microchannel. *J Power Sources* 2006;159:810-6. DOI
17. Wilcox G, Mitchell P. Electrolyte additives for zinc-anoded secondary cells I. Brighteners, levellers and complexants. *J Power Sources* 1989;28:345-59. DOI
18. Tao H, Lian C, Liu H. Multiscale modeling of electrolytes in porous electrode: from equilibrium structure to non-equilibrium transport. *Green Energy Environ* 2020;5:303-21. DOI
19. Parker JF, Chervin CN, Nelson ES, Rolison DR, Long JW. Wiring zinc in three dimensions re-writes battery performance - dendrite-free cycling. *Energy Environ Sci* 2014;7:1117-24. DOI
20. Liu J, Guan C, Zhou C, et al. A flexible quasi-solid-state nickel-zinc battery with high energy and power densities based on 3D electrode design. *Adv Mater* 2016;28:8732-9. DOI PubMed
21. Banik SJ, Akolkar R. Suppressing dendrite growth during zinc electrodeposition by PEG-200 additive. *J Electrochem Soc* 2013;160:D519-23. DOI
22. Wang J, Zhang L, Zhang C, Zhang J. Effects of bismuth ion and tetrabutylammonium bromide on the dendritic growth of zinc in alkaline zincate solutions. *J Power Sources* 2001;102:139-43. DOI
23. Mansfeld F, Gilman S. The effect of lead ions on the dissolution and deposition characteristics of a zinc single crystal in 6N KOH. *J Electrochem Soc* 1970;117:588. DOI
24. Wang SB, Ran Q, Yao RQ, et al. Lamella-nanostructured eutectic zinc-aluminum alloys as reversible and dendrite-free anodes for aqueous rechargeable batteries. *Nat Commun* 2020;11:1634. DOI PubMed PMC
25. Qi Z, Xiong T, Yu ZG, et al. Suppressing zinc dendrite growth in aqueous battery via Zn-Al alloying with spatially confined zinc reservoirs. *J Power Sources* 2023;558:232628. DOI
26. Peng Y, Lai C, Zhang M, et al. Zn-Sn alloy anode with repressible dendrite grown and meliorative corrosion resistance for Zn-air battery. *J Power Sources* 2022;526:231173. DOI
27. Xue R, Kong J, Wu Y, et al. Highly reversible zinc metal anodes enabled by a three-dimensional silver host for aqueous batteries. *J Mater Chem A* 2022;10:10043-50. DOI
28. Tao H, Hou Z, Zhang L, Yang X, Fan L. Manipulating alloying reaction to achieve the stable and dendrite-free zinc metal anodes. *Chem Eng J* 2022;450:138048. DOI
29. Fayette M, Chang HJ, Li X, Reed D. High-performance InZn alloy anodes toward practical aqueous zinc batteries. *ACS Energy Lett* 2022;7:1888-95. DOI
30. Sun K, Xiao Z, Shen Y, et al. MOF-derived Se doped $MnS/Ti_3C_2T_x$ as cathode and Zn- $Ti_3C_2T_x$ membrane as anode for rocking-chair zinc-ion battery. *Nano Res* 2024;17:2781-9. DOI
31. Shen Y, Liu Y, Sun K, et al. Zincophilic $Ti_3C_2Cl_2$ MXene and anti-corrosive Cu NPs for synergistically regulated deposition of dendrite-free Zn metal anode. *J Mater Sci Technol* 2024;169:137-47. DOI
32. Mcbreen J, Gannon E. The electrochemistry of metal oxide additives in pasted zinc electrodes. *Electrochimica Acta* 1981;26:1439-46. DOI
33. Sun K, Shen Y, Min J, et al. MOF-derived Zn/Co co-doped MnO/C microspheres as cathode and $Ti_3C_2@Zn$ as anode for aqueous zinc-ion full battery. *Chem Eng J* 2023;454:140394. DOI
34. Cheng XB, Zhang R, Zhao CZ, Zhang Q. Toward safe lithium metal anode in rechargeable batteries: a review. *Chem Rev* 2017;117:10403-73. DOI PubMed
35. Zheng X, Ahmad T, Chen W. Challenges and strategies on Zn electrodeposition for stable Zn-ion batteries. *Energy Storage Mater* 2021;39:365-94. DOI
36. Zhao Q, Liu W, Chen Y, Chen L. Ultra-stable Zn metal batteries with dendrite-free Cu-Sn alloy induced high-quality composite Zn mesh. *Chem Eng J* 2022;450:137979. DOI
37. Zhang Y, Howe JD, Ben-yoseph S, Wu Y, Liu N. Unveiling the origin of alloy-seeded and nondendritic growth of Zn for rechargeable aqueous Zn batteries. *ACS Energy Lett* 2021;6:404-12. DOI
38. Chen Z, Yang Y. Data-driven design of eutectic high entropy alloys. *J Mater Inf* 2023;3:10. DOI
39. Hu Y, Chen J, Wei Z, He Q, Zhao Y. Recent advances and applications of machine learning in electrocatalysis. *J Mater Inf* 2023;3:18. DOI
40. Wang Y, Wagner N, Rondinelli JM. Symbolic regression in materials science. *MRS Commun* 2019;9:793-805. DOI
41. Ouyang R, Curtarolo S, Ahmetcik E, Scheffler M, Ghiringhelli LM. SISSO: a compressed-sensing method for identifying the best low-

- dimensional descriptor in an immensity of offered candidates. *Phys Rev Mater* 2018;2:083802. DOI
42. Weng B, Song Z, Zhu R, et al. Simple descriptor derived from symbolic regression accelerating the discovery of new perovskite catalysts. *Nat Commun* 2020;11:3513. DOI PubMed PMC
 43. Kresse G, Hafner J. *Ab initio* molecular dynamics for liquid metals. *Phys Rev B Condens Matter* 1993;47:558-61. DOI PubMed
 44. Kresse G, Hafner J. *Ab initio* molecular-dynamics simulation of the liquid-metal-amorphous-semiconductor transition in germanium. *Phys Rev B Condens Matter* 1994;49:14251-69. DOI PubMed
 45. Kresse G, Furthmüller J. Efficient iterative schemes for *ab initio* total-energy calculations using a plane-wave basis set. *Phys Rev B Condens Matter* 1996;54:11169-86. DOI PubMed
 46. Kresse G, Furthmüller J. Efficiency of *ab-initio* total energy calculations for metals and semiconductors using a plane-wave basis set. *Comput Mater Sci* 1996;6:15-50. DOI
 47. Perdew JP, Burke K, Wang Y. Generalized gradient approximation for the exchange-correlation hole of a many-electron system. *Phys Rev B Condens Matter* 1996;54:16533-9. DOI PubMed
 48. Zhou F, Cococcioni M, Marianetti CA, Morgan D, Ceder G. First-principles prediction of redox potentials in transition-metal compounds with LDA + *U*. *Phys Rev B* 2004;70:235121. DOI
 49. Monkhorst HJ, Pack JD. Special points for Brillouin-zone integrations. *Phys Rev B* 1976;13:5188-92. DOI
 50. Zheng J, Zhao Q, Tang T, et al. Reversible epitaxial electrodeposition of metals in battery anodes. *Science* 2019;366:645-8. DOI PubMed
 51. Cai Z, Wang J, Lu Z, et al. Ultrafast metal electrodeposition revealed by in situ optical imaging and theoretical modeling towards fast-charging Zn battery chemistry. *Angew Chem Int Ed Engl* 2022;61:e202116560. DOI PubMed
 52. Jain A, Ong SP, Hautier G, et al. Commentary: the materials project: a materials genome approach to accelerating materials innovation. *APL Mater* 2013;1:011002. DOI
 53. Wagner S, Kronberger G, Beham A, et al. Architecture and design of the heuristiclab optimization environment. In: Klempous R, Nikodem J, Jacak W, Chaczko Z, editors. *Advanced methods and applications in computational intelligence*. Heidelberg: Springer International Publishing; 2014. pp. 197-261. DOI
 54. Liu Z, Ren J, Wang F, et al. Tuning surface energy of Zn anodes via Sn heteroatom doping enabled by a codeposition for ultralong life span dendrite-free aqueous Zn-ion batteries. *ACS Appl Mater Interfaces* 2021;13:27085-95. DOI PubMed
 55. Jäckle M, Helmbrecht K, Smits M, Stottmeister D, Groß A. Self-diffusion barriers: possible descriptors for dendrite growth in batteries? *Energy Environ Sci* 2018;11:3400-7. DOI
 56. Huang K, Liu Y, Liu H. Understanding and predicting lithium crystal growth on perfect and defective interfaces: a kohn-sham density functional study. *ACS Appl Mater Interfaces* 2019;11:37239-46. DOI PubMed
 57. Kim HJ, Kim S, Kim S, et al. Gold-nanolayer-derived zincophilicity suppressing metallic zinc dendrites and its efficacy in improving electrochemical stability of aqueous zinc-ion batteries. *Adv Mater* 2024;36:e2308592. DOI
 58. Yu J, Xi S, Pan S, et al. Machine learning-guided design and development of metallic structural materials. *J Mater Inf* 2021;1:9. DOI
 59. Pei W, Zhang W, Yu X, et al. Computational design of spatially confined triatomic catalysts for nitrogen reduction reaction. *J Mater Inf* 2023;3:26. DOI